

Electromagnetic transitions and structure of ^{46}Ti

F. Brandolini,¹ J. R. B. Oliveira,² N. H. Medina,² R. V. Ribas,² J. Sanchez-Solano,³ D. Bucurescu,⁴ S. M. Lenzi,¹
C. A. Ur,^{1,4} D. Bazzacco,¹ M. De Poli,⁵ E. Farnea,¹ A. Gadea,⁵ N. Marginean,^{4,5} and C. Rossi-Alvarez¹

¹*Dipartimento di Fisica and INFN, Padova, Italy*

²*Instituto de Física, Universidade de São Paulo, São Paulo, Brasil*

³*Departamento de Física Teórica, Universidad Autónoma, Cantoblanco, Madrid, Spain*

⁴*National Institute for Physics and Nuclear Engineering, Bucharest, Romania*

⁵*INFN, Laboratori Nazionali di Legnaro, Legnaro, Italy*

(Received 4 March 2004; published 7 September 2004)

The nucleus ^{46}Ti has been studied with the reaction $^{24}\text{Mg}(^{28}\text{Si}, \alpha 2p)^{46}\text{Ti}$, at the bombarding energy of 115 MeV. Thin target foils backed either with Au or Pb layers were used in order to perform DSAM lifetime measurements. The yrast 13^- , 14^- , and 15^- levels were found to depopulate towards a sideband with enhanced stretched M1 transitions. The deduced B(E2) and B(M1) rates for the bands with $K=0^+$ and 3^- agree in general with the values predicted by the Large Scale Shell Model. As a complementary information, the lifetimes of the yrast 4^+ states in ^{48}Cr and ^{50}Cr have been measured in the reactions $^{24}\text{Mg}(^{28}\text{Si}, 2p2n)^{48}\text{Cr}$ and $^{26}\text{Mg}(^{28}\text{Si}, 2p2n)^{50}\text{Cr}$ and found to agree with Shell Model predictions.

DOI: 10.1103/PhysRevC.70.034302

PACS number(s): 21.10.Tg, 21.60.Cs, 23.20.Lv, 27.40.+z

I. INTRODUCTION

In recent years an extensive experimental research has been carried out at the Legnaro National Laboratories (LNL) in the nuclei $^{48,49,50}\text{Cr}$ and $^{46,47,48}\text{V}$, lying in the middle of the $1f_{7/2}$ shell, with the major aim to get reliable experimental B(E2) values in order to investigate the rotational collectivity. For this purpose the lifetimes of several levels have been determined with a careful Doppler shift attenuation method (DSAM) analysis [1–6]. Large scale shell model (LSSM) calculations in the full pf configuration space [7] reproduce very well the excitation energies of the observed natural parity levels and the transition probabilities, while the unnatural parity bands are well reproduced by extending the configuration space to include a $d_{3/2}$ -hole. Prolate deformation configurations are generated at low excitation energy, which can be classified in the framework of the Nilsson model. The attention was focused on the yrast sequence of levels up to the spherical band termination in the $1f_{7/2}^n$ and $1d_{3/2}^{-1} \otimes 1f_{7/2}^{n+1}$ configuration spaces, for natural parity and unnatural parity, respectively. These bands are selectively populated in heavy-ion induced fusion reactions.

In the present work the ^{46}Ti nucleus is studied. At the time of a recent review [8], this nucleus turned out to have been studied at low excitation energy with different techniques, but that the knowledge at high spin was rather sparse. More recently, using the reaction $^{28}\text{Si}(^{24}\text{Mg}, \alpha 2p)$ at 115 MeV on a thin self-supporting target, the ^{46}Ti states were reported beyond band termination at 14^+ for the ground-state (gs) band and beyond the terminating level 17^- for a $K=3^-$ band [9], greatly extending the level scheme with respect to a similar heavy ion study [10]. The latter band is explained as due to a proton promotion from the $[202]3/2^+$ Nilsson orbital to the $[321]3/2^-$ one, followed by parallel coupling of the unpaired spins. A classification according to the quantum number K is anyhow reasonable only for the lowest states of the bands because the deformation decreases strongly approaching the band termination.

DSAM lifetimes will be presented which allow to extend the understanding of this nucleus. Preliminary data have been presented in Ref. [11].

A condition to get this improvement is to adopt reliable stopping power curves. The ^{46}Ti nucleus is particularly suited for stopping power calibration since lifetimes of low-lying levels are well known. In fact, after the last compilation [8] further precise lifetimes obtained with the recoil distance Doppler shift (RDDS) method became available [12]. One can thus adjust the stopping power in a DSAM line shape analysis in order to get the best fit when adopting well known lifetime values. Both Au and Pb were employed as stopping materials. The use of Pb is to be preferred in the case of long-lived transitions since the Doppler broadening is enhanced, due to the nearly two times smaller stopping power.

The second experimental part of this work is aimed to get more precise lifetime values for the long lived 4^+ states in ^{48}Cr and ^{50}Cr , using the adjusted stopping power curves for Pb backing. ^{48}Cr is crucial for understanding the structure of the $1f_{7/2}$ nuclei as its gs band is predicted by LSSM to have the largest deformation in this region. This is currently assumed but it is not fully proved experimentally, since the lifetimes of low-lying levels were obtained in DSAM experiments with large error bars, rising to about 30% for the 4^+ level [1], therefore not very restrictive.

II. EXPERIMENTAL PROCEDURE

The nuclei ^{46}Ti , ^{48}Cr , and ^{50}Cr have been populated with the reactions $^{24}\text{Mg}(^{28}\text{Si}, \alpha 2p)^{46}\text{Ti}$, $^{24}\text{Mg}(^{28}\text{Si}, 2p2n)^{48}\text{Cr}$, and $^{26}\text{Mg}(^{28}\text{Si}, 2p2n)^{50}\text{Cr}$, respectively, at 115 MeV bombarding energy. The beams were provided by LNL 15 MV XTU-tandem. The target consisted of a 0.8 mg/cm² foil with either thick Au or Pb backing of 10 mg/cm².

The γ rays were detected with the γ -detector array GASP, comprising 40 Compton-suppressed HPGe detectors and a

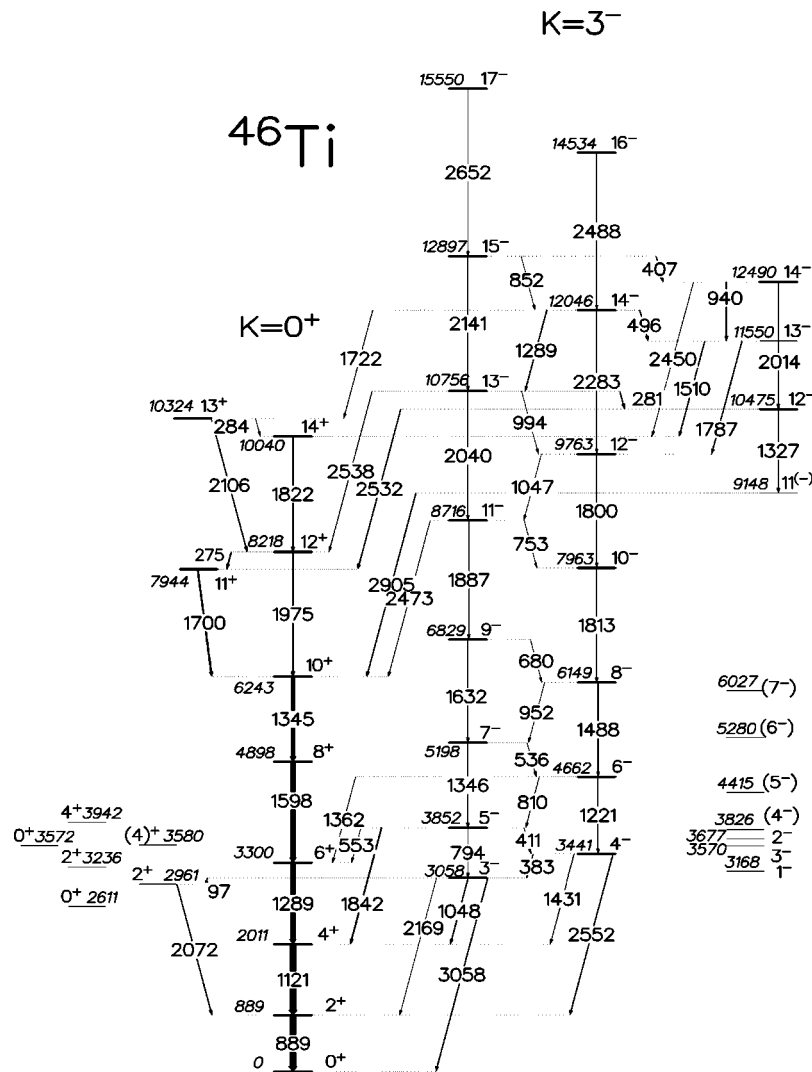


FIG. 1. Adopted level scheme of ^{46}Ti .

80-element BGO ball which acts as a γ -ray multiplicity filter.

In order to allow the lifetime analysis, data were sorted into seven γ - γ matrices having on the first axis the detectors in rings at 34° , 60° , 72° , 90° , 108° , 120° , 146° and on the second axis any of the other 39 detectors. Events were stored on tape when at least two Ge detectors and two elements of the multiplicity filter fired in coincidence. The same procedure has been used in previous works [5].

III. EXPERIMENTAL RESULTS

A. The ^{46}Ti level scheme

A level scheme of ^{46}Ti , updated with respect to the last $A=46$ Nuclear Data Sheets [8], is shown in Fig. 1. In the present experiment no new levels were found with respect to a previous one [9].

Positive parity levels are displayed only up to the yrast level $I^\pi=14^+$, the band termination in the $1f_{7/2}^n$ shell, because above it their lifetimes are below the DSAM sensitivity range. Several positive parity low-spin levels are known [8], which were not significantly populated with the present re-

action. Those at low energy and measured in more than one experiment are reported in leftmost part of Fig. 1 in tentative bands. Only γ -transitions observed in the present experiment are reported.

The members of the $K=3^-$ band are reported up to 17^- , the terminating state in the $1d_{3/2}^{-1}1f_{7/2}^{n+1}$ configuration space. The levels above the yrast 11^- state were taken from Ref. [9]. The levels at 9148, 10 475, 11 550, and 12 490 keV are taken from the same reference, with the spin-parity assignment deduced from the present lifetime measurements. Further low-spin negative parity levels [8,13], not efficiently observed in this experiment are grouped on the rightmost part of Fig. 1, but they will be not extensively discussed in this work. The spin assignments of Ref. [13], recently confirmed in Ref. [14], are adopted for levels at 3826, 4415, 5280, and 6027 keV. The transitions from the 7^- level (at 5198 keV) to the one at 3826 keV and from the 8^- level (at 6149 keV) to the one at 4415 keV, reported in [15], were not observed. On the other hand, they were not confirmed in successive experiments, including one with the same first author [10].

TABLE I. Experimental and theoretical results in ^{46}Ti . Errors in γ -ray-energies are 0.3 keV when a decimal is quoted, otherwise 1 keV. Not observed gammas are given in brackets. The lifetime values refer to the upper level of the transition.

Transition $I_i^\pi \rightarrow I_f^\pi$	E_γ expt. (keV)	E_γ SM (keV)	γ -BR expt. (%)	τ expt. (ps)	τ previous (ps)	B(E2) expt. ($e^2 \text{ fm}^4$)	B(E2) th. ($e^2 \text{ fm}^4$)	B(M1) expt. (μ_N^2)	B(M1) th. (μ_N^2)
$K=0^+$									
$2^+ \rightarrow 0^+$	889.3	993	100		7.63(7) ^c	191(2) ^c	116		
$4^+ \rightarrow 2^+$	1120.6	898	100	2.01(23)	2.34(14) ^b 2.00(15) ^c	231(27)	154		
$6^+ \rightarrow 4^+$	1289.4	1135	100	1.34(13)	1.43(13) ^b	170(17)	154		
$8^+ \rightarrow 6^+$	1598.0	1543	100	0.51(5)	0.64(10) ^b	154(15)	140		
$10^+ \rightarrow 8^+$	1345.4	1414	100	1.68(15)		110(10)	101		
$11^+ \rightarrow 10^+$	1700.3	1689	100	<0.05			0.2	>0.15	0.44
$12^+ \rightarrow 10^+$	1975.1	2097	65(3)	0.42(5)		42(5)	41		
$12^+ \rightarrow 11^+$	275.1	408	35(3)	0.42(5)			18	2.23(21)	1.87
$13^+ \rightarrow 12^+$	2106	2168	96(1) ^a	0.06(2)			0.03	0.10(3)	0.10
$13^+ \rightarrow 14^+$	284	150	4(1) ^a	0.06(2)			3	2.0(7)	2.82
$14^+ \rightarrow 12^+$	1821.6	2017	100	1.10(10)		37(4)	35		
$K=3^-$									
$4^- \rightarrow 3^-$	383.0	179	77(2)		106.6(5) ^c		356	0.007(1)	0.02
$5^- \rightarrow 3^-$	793.9	691	11.5(22)		6.9(12) ^b	43(10)	59		
$5^- \rightarrow 4^-$	411.3	511	3.9(14)				289	0.005(2)	0.00
$6^- \rightarrow 4^-$	1220.8	1344	71(5)	1.22(13)	1.5(3) ^c	177(23)	142		
$6^- \rightarrow 5^-$	809.7	833	20.5(45)				166	0.018(4)	0.03
$7^- \rightarrow 5^-$	1345.5	1336	97(1)	0.80(9)		225(26)	193		
$7^- \rightarrow 6^-$	536.1	504	3(1)				166	0.015(10)	0.02
$8^- \rightarrow 6^-$	1487.6	1376	97(1)	0.48(6)		227(28)	189		
$8^- \rightarrow 7^-$	952	872	3(1)				87	0.004(2)	0.03
$9^- \rightarrow 7^-$	1631.9	1552	89(3)	0.29(4)		220(31)	201		
$9^- \rightarrow 8^-$	680	680	11(3)				86	0.070(21)	0.02
$10^- \rightarrow 8^-$	1813.4	1844	100	0.23(4)		181(29)	156		
$10^- \rightarrow 9^-$	(1132)	1165	<2				25	<0.01	0.00
$11^- \rightarrow 9^-$	1887.4	1677	71(5)	0.15(3)		164(31)	171		
$11^- \rightarrow 10^-$	753	512	6(2)				71	0.055(20)	0.00
$12^- \rightarrow 10^-$	1800.0	1992	97(1)	0.23(4)		186(30)	139		
$12^- \rightarrow 11^-$	1047	1480	3(1)				10	0.006(4)	0.00
$13^- \rightarrow 11^-$	2040	2072	67(5)	0.10(2)		104(27)	169		
$13^- \rightarrow 12^-$	994	592	9(2)				32	0.054(17)	0.03
$13^- \rightarrow 12_2^-$	281	29	4(1)				23	1.09(42)	0.87
$14^- \rightarrow 12^-$	2283	2425	39(7)	0.10(3)		59(21)	67		
$14^- \rightarrow 13^-$	1289	1832	19(6)				8	0.06(3)	0.00
$14^- \rightarrow 13_2^-$	496	772	16(2)				16	0.7(3)	1.14
$15^- \rightarrow 13^-$	2141	2214	70(5)	0.14(3)		110(22)	125		
$15^- \rightarrow 14^-$	852	381	10(4)				43	0.06(3)	0.11
$15^- \rightarrow 14_2^-$	407	144	20(5)				4	1.04(35)	1.72
$16^- \rightarrow 14^-$	2488	2669	100	0.15(3)		58(10)	49		
$16^- \rightarrow 15^-$	(1631)	2288	<5				3	<0.01	0.01
$16^- \rightarrow 15_2^-$		757					1		0.32
$17^- \rightarrow 15^-$	2652	2752	100	0.10(2)	62(14)	64			
$17^- \rightarrow 16^-$	(1017)	464	<6				32	<0.05	0.00
$17^- \rightarrow 16_2^-$		-709					9		2.95

^aReference [9].^bReference [8].^cReference [12].

TABLE II. Lifetimes from the analysis of stretched E2 transitions in the gs band of ^{46}Ti . In order to evaluate the systematic error, present errors are only statistic. The lifetime values refer to the upper level of the transition.

Transition $I_i^\pi \rightarrow I_f^\pi$	E_γ (keV)	Au backing (ps)	Pb backing (ps)	Previous (ps)
$2^+ \rightarrow 0^+$	889			7.63(7) ^a
$4^+ \rightarrow 2^+$	1121		2.01(10)	2.18(11) ^a
$6^+ \rightarrow 4^+$	1289	1.35(7)	1.32(8)	1.43(13)
$8^+ \rightarrow 6^+$	1598	0.51(4)	0.50(5)	0.64(10)
$10^+ \rightarrow 8^+$	1345	1.66(6)	1.70(7)	
$12^+ \rightarrow 10^+$	1975	0.42(4)	0.41(5)	
$14^+ \rightarrow 12^+$	1822	1.08(5)	1.12(6)	

^aAverage of Refs. [8,12]

Experimental energies and branching ratios are presented in Table I for transitions without parity change, while those for transitions with parity change are postponed to Table III. Unless differently reported, branching ratios from present data are adopted, which are in general consistent with data of Ref. [9].

B. Lifetimes in ^{46}Ti

The program LINESHAPE [16] was used to get lifetime estimates from line shape analysis. The Northcliffe-Schilling stopping power [17], corrected for atomic shell effects [18], was used. The original code was modified in order to allow the narrow gate on transition below (NGTB) procedure [19], which is free from systematic errors related with sidefeeding uncertainties. More details about the analysis procedure are reported in Ref. [1].

The results for the lifetimes of the even- I levels in the gs band are presented in Table II. They were obtained with the NGTB procedure, apart for the 14^+ terminating state. A first example of the NGTB analysis is shown in Fig. 2 for the lifetime determination of the yrast 4^+ level in ^{46}Ti , which decays to the 2^+ level with a 1121 keV γ -transition. Taking a transition populating the level under study as a probe, the lifetime of the level is provided by the comparison of its full line shape with the partly suppressed line shape, obtained with a narrow gate on a Doppler broadened transition depopulating the level. Owing to the particularly long lifetime, the measurement could be made only using Pb.

In order to check the size of systematic errors, caused by the adopted stopping power, the errors quoted in Table II are only statistical. The lifetime determination for the 6^+ level, using a Au backing, agrees well with the precise published value, determined also with Coulomb excitation [8]. This was already considered in Ref. [1] for Cr is Au, to which we refer for a detailed discussion, and therefore the same systematic error of 8% is assumed there, in the subsequent works in neighboring nuclei [2–6] and in the present work. As reported in Table II, similar lifetime values as in Au were obtained with Pb backing when a reduction of 10% is applied the stopping power of Ref. [18], which was thus adopted in this work. The adjusted lifetime values depart statistically from the ones with Au backing by 5%–6% on the

average. This error is quadratically added to the 8% adopted for Au getting approximately 10%. Such systematic errors were applied to the lifetimes reported in Tables I and III. For lifetimes shorter than 0.4 ps the determination with Au backing is reported, while for the longer ones an average was taken of the determinations with Au and Pb backings.

The lifetimes of the gs band levels were obtained consecutively from the top to the bottom of the cascade. The probe transition line shapes were fitted by varying the side-

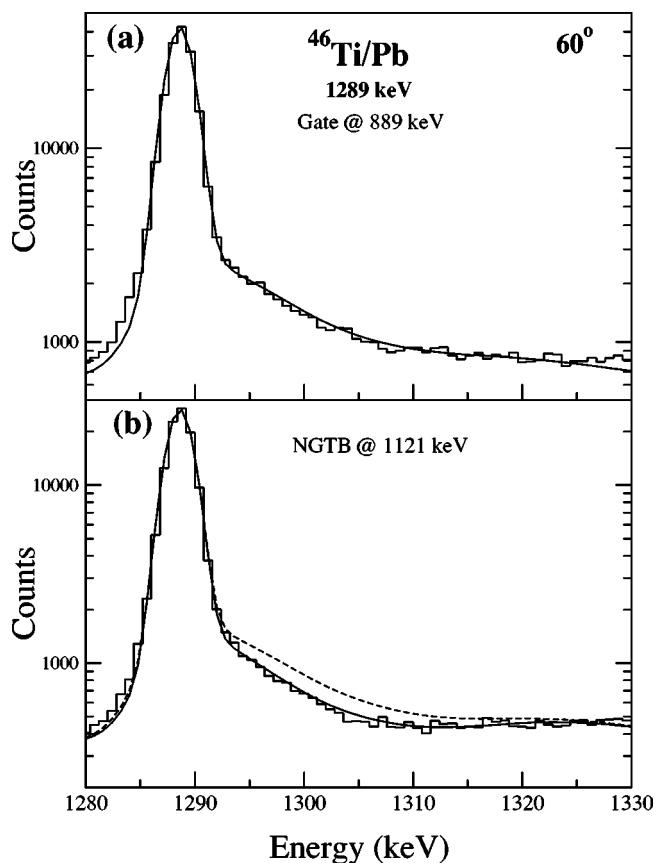


FIG. 2. NGTB analysis of the $4^+ \rightarrow 2^+$ 1121 keV transition in ^{46}Ti , using the 1289 keV line as a probe. The γ lines were analyzed at 60° and gated at (a) 889 keV (wide) and (b) 1121 keV (narrow). The dashed line in (b) displays the full line shape which corresponds to the fit in (a).

TABLE III. Results for parity changing transitions in ^{46}Ti . The lifetime values refer to the upper level of the transition.

Transition $I_i^\pi \rightarrow I_f^\pi$	E_γ (keV)	M	BR (%)	τ (ps)	W.u.
$3^- \rightarrow 2^+$	2169.3	E1	1.5(5)	31.3(5) ^b	$1.8(6) \cdot 10^{-5}$
$3^- \rightarrow 4^+$	1048.7	E1	97.0(9)	31.3(5)	$2.1(1) \cdot 10^{-5}$
$3^- \rightarrow 2_2^+$	97	E1	0.12(4)	31.3(5)	$0.54(15) \cdot 10^{-5}$
$3^- \rightarrow 0^+$	3058.4	E3	1.4(2)	31.3(5)	2.6(4)
$4^- \rightarrow 4^+$	1431.4	E1	22(2)	106.6(5) ^b	$0.05(1) \cdot 10^{-5}$
$4^- \rightarrow 2^+$	2552	M2+(E3)	1.0(2)	106.6(5)	0.04(1)
$5^- \rightarrow 4^+$	1842.4	E1	80(3)	6.9(12) ^a	$1.3(5) \cdot 10^{-5}$
$5^- \rightarrow 6^+$	553.2	E1	4.6(8)	6.9(12)	$2.8(6) \cdot 10^{-5}$
$6^- \rightarrow 6^+$	1362	E1	8.5(8)	1.25(13) ^a	$2.0(3) \cdot 10^{-5}$
$11^- \rightarrow 10^+$	2473	E1	23(5)	0.15(3) ^a	$7.8(21) \cdot 10^{-5}$
$13^- \rightarrow 12^+$	2538	E1	23(5)	0.10(2) ^a	$18(7) \cdot 10^{-5}$
$14^- \rightarrow 13^+$	1722	E1	26(8)	0.10(2) ^a	$39(10) \cdot 10^{-5}$

^aPresent work.^bReference [12].

feeding times, adopting the values for the upper lying states from the prior analysis. For each state, the probe transition was a direct feeder with the exception of the lifetime of the ($I^\pi=6^+$) state, for which the probe transition was the 1345 keV line (using the ($I^\pi=8^+$) state lifetime previously determined). In most cases some minor contaminant transitions were taken into account improving the fit quality, but the lifetime results are only mildly affected by these corrections. The NGTB analyses for the 12^+ level in both Au and Pb measurements are shown in Fig. 3.

The lifetime of the band terminating state ($I^\pi=14^+$) was obtained from a standard DSAM analysis of the 1822 keV line shape. Its full line shape (upper part of Fig. 3) was obtained setting a broad gate on the 1289 keV transition, since the spectra gated on a lower and narrower transition would be strongly contaminated by the 1813 keV transition belonging to the $K^\pi=3^-$ band. The line shapes were fitted simultaneously for detectors placed at the seven angles of the GASP array and all the results are of similar quality as that shown in Fig. 3. The analysis is unambiguous since the line shape has been fitted essentially with a single lifetime, once the sidefeeding is very fast. The weighted averages from determinations using Pb and Au backing are reported in Table I. The stretched $\Delta I=1$ transitions from the 11^+ and 13^+ levels, assigned in Fig. 1 to the gs band, have been analyzed in the standard way using the Au backing. The $11^+ \rightarrow 10^+$, 1700 keV, transition turned out to be very fast (<0.05 ps) in accordance with Ref. [10] and in disagreement with Ref. [8].

The lifetimes for the levels of the negative parity band with ($K^\pi=3^-$) were obtained by standard DSAM analysis with Au backing. For the even spin states the line shapes were fitted considering the 1842 keV gated spectrum while for the odd spin states the line shapes were fitted to the 383 keV gate spectrum and are reported in Table I. The experimental B(M1) values for the stretched decay from the yrast levels 13^- and 15^- towards nonyrast levels turned out to be very large. The standard line shape analysis for $9^- \rightarrow 7^-$, 1632 keV, and $8^- \rightarrow 6^-$, 1488 keV transitions are shown in Fig. 4.

C. Lifetimes in ^{48}Cr and ^{50}Cr

The lifetimes for the yrast 4^+ levels in ^{48}Cr and ^{50}Cr were determined with the NGTB procedure in the measurement with Pb backing. Typical examples of line shape analysis are shown in Fig. 5, leading to the lifetime values 1.74(18) and 2.12(23) ps for ^{48}Cr and ^{50}Cr , respectively. The aforementioned stopping power correction for Pb was applied. The uncertainties were sensibly reduced with respect to those previously reported [1].

IV. DISCUSSION

A. Positive parity levels in ^{46}Ti

The experimental positive parity levels are compared with the theoretical ones in Fig. 6. Only the lowest 0^+ , 2^+ , and 4^+ levels are considered in addition to the gs band. The calculations were made with the code ANTOINE in the full fp shell, adopting the KB3 interaction [7]. Rather good agreement was achieved for the gs band. Alternative calculations were also made using the KB3G interaction [20], just a slightly modified version designed for nuclei approaching ^{56}Ni , with negligible variations. In fact, in Ref. [20] it is remarked that the interactions KB3 and KB3G give equivalent results in the middle of the shell, being the variations of the transition rate values limited to a few percent. Also the effective interaction FPD6 [21] is frequently used in this region, but, for nuclei in the middle of the $1f_{7/2}$ shell, often results in B(E2) values up to 20% too large when compared with experimental values, as in the case of the yrast bands analyzed in Refs. [1–6], which are, on the other hand, well explained by the KB3/KB3G ones. For this reason those predictions are not considered further here.

Concerning the decay properties, it is confirmed that the experimental lifetime of the yrast 4^+ in ^{46}Ti is sensibly shorter than the calculated one, similarly to what occurs for the level 2^+ [8]. This is ascribed to some contribution of deformed 2-hole and 4-hole configurations in the sd shell,

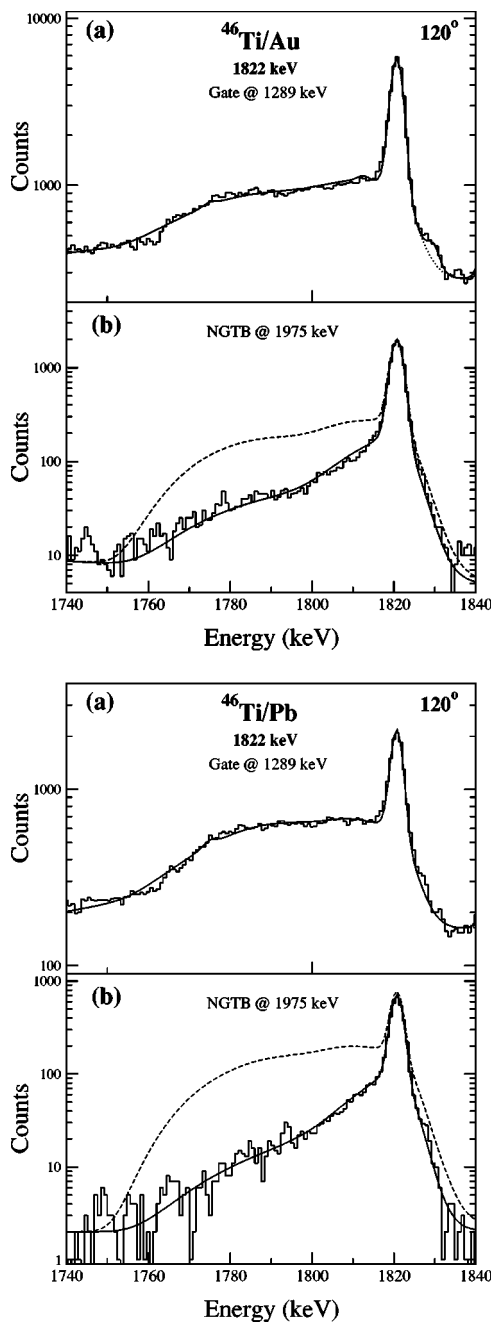


FIG. 3. DSAM line shape fits for the 1822 keV transition in ^{46}Ti at 120° . (a) Standard analysis for the terminating level 14^+ and (b) NGTB at the 1975 keV transition for the measurement of the 12^+ state lifetimes. Left: data with Au backing. Right: data with Pb backing.

very important at the beginning of the $1f_{7/2}$ shell [22]. Such interpretation is confirmed by the consideration that the second 0^+ level is most probably an intruder level with respect to the pf configuration space since it is positioned at 2611 keV while it is predicted by LSSM in the full pf configuration space to lie above 4 MeV. It is thus candidate to be the head of a deformed band having mostly a $2h$ - and $4h$ -configuration, which somewhat mixes with the lowest levels of the gs band. Similar conclusions were recently obtained for ^{44}Ti [23], in which case the yrare 0^+ lies at 1907 keV and

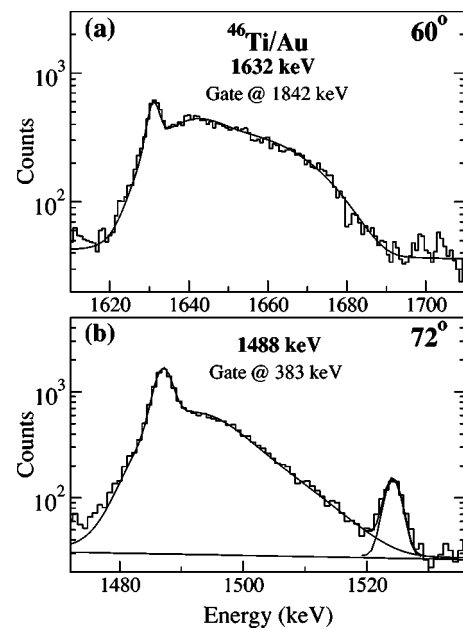


FIG. 4. Standard line shape analysis of the (a) $9^- \rightarrow 7^-$ 1632 keV transition at 60° (gate at 1842 keV) and (b) of the $8^- \rightarrow 6^-$ 1488 keV transition at 72° (gate at 383 keV) in ^{46}Ti . Data from Au backing experiment.

a 45% admixture is evaluated for the ground state. The higher excitation in ^{46}Ti leads to the expectation of a lower but still relevant mixing. In contrast to that, the yrare 0^+ at 3694 keV in the cross-conjugate ^{50}Cr is rather well reproduced (i.e., 3950 keV), likely because with increasing mass the hole configurations become less important.

Experimental results for positive parity levels are compared with theory in the upper part of Table I, while the $B(E2)$ values are shown in Fig. 7. Standard effective charges $0.5e$ and $1.5e$ are assumed for valence neutrons and protons, respectively. An estimate of the transition quadrupole moment Q_t can be obtained from the $B(E2)$ value of the 6^+ level, using the rotational model. A deformation parameter $\beta \approx 0.22$ is estimated with the formula [24]: $Q_t = 1.09ZA^{2/3}\beta(1+0.36\beta) \text{ fm}^2$.

$B(M1)$ values are reported for transitions $12^+ \rightarrow 11^+$, $13^+ \rightarrow 12^+$, and $13^+ \rightarrow 14^+$. The first and the last $B(M1)$ values are very large, while the second one is small. This staggering reflects the dominance of $1f_{7/2}^n$ configurations approaching the band termination [25].

The gs band in ^{46}Ti is rotorlike up to $I^\pi = 8^+$, while above it experiences a backbending and the 12^+ decays with a fast M1 to a 11^+ level. LSSM does not interpret this as a band-crossing since the yrare 10^+ is expected 1.3 MeV above the yrast one. For an alternative explanation, it was observed in the introduction that a K classification is valid only at low spin. This is particularly stringent in ^{46}Ti , since it is not a very deformed nucleus. The backbending at 10^+ can be related to an intrinsic and abrupt change from collective to noncollective regime, as probably occurs also in ^{48}Cr , but with a delayed backbending at $I^\pi = 12^+$. It is relevant to note that the situation is different in the cross-conjugate nucleus ^{50}Cr . There, the yrast 10^+ level, lower by 414 keV than the

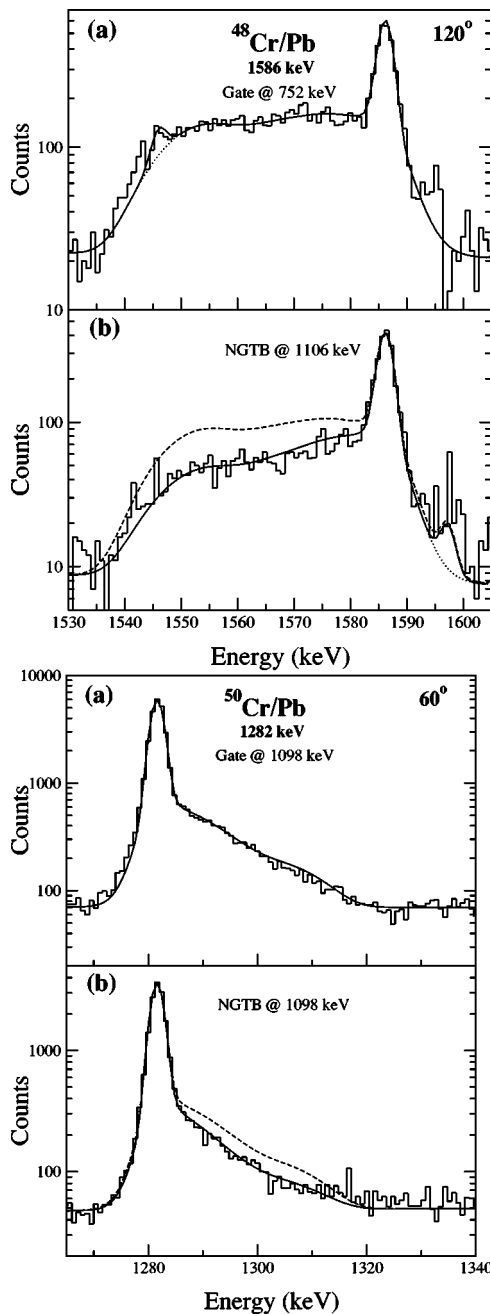


FIG. 5. (Left) NGTB analysis of the 4^+ level in ^{48}Cr using the $6^+ \rightarrow 4^+$ 1586 keV transition as a probe at 120° , (a) 752 keV gate and (b) 1106 keV narrow gate. (Right) NGTB analysis of the 4^+ level in ^{50}Cr using the $6^+ \rightarrow 4^+$ 1282 keV transition as a probe at 60° , (a) 1098 keV gate and (b) 1098 keV narrow gate.

rarer one, is the head of $K^\pi=10^+$ band, which is due to the simultaneous breaking of neutron and proton pairs with a recoupling of the four nucleons to the maximum value of angular momentum [14]. Owing to the active Nilsson orbitals in ^{46}Ti , the band obtained in a similar way has about the same excitation energy but $K=6$ and thus would be largely nonyrast.

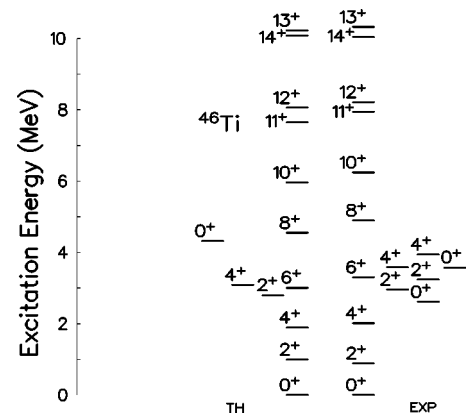


FIG. 6. Comparison between experimental and theoretical positive parity levels in ^{46}Ti , assuming the KB3 effective interaction.

B. Negative parity levels in ^{46}Ti

As summarized in Table I, the yrast 13^- , 14^- , and 15^- levels at 10 756, 12 046, and 12 897 keV, respectively, decay partially via 281, 496, and 407 keV γ -ray to nonyrast $I=12$, 13, and 14 levels. For a positive parity assignment, this implies in all cases an E1 strength largely exceeding the adopted E1 limit of $3 \cdot 10^{-4}$ W.u. in this nuclear region [2], so that stretched M1 decays are assigned to these transitions and thus a negative parity to the fed levels.

Experimental negative parity levels are compared with calculated ones in Fig. 8. The agreement is in general satisfactory for the $K=3^-$ band, but it must be stressed that the members of the even spin signature are predicted too high by about 300 keV for levels 12^- , 14^- , and 16^- , indicating that some structural effects are not well described.

In the present calculations the configuration space was extended to include a nucleon-hole in the $d_{3/2}$ orbital and the same effective interaction as for ^{47}V [26] was used, together with standard binding energies. In the case of unnatural parity levels the choice of the effective interaction is more difficult. In previous calculations with the code ANTOINE, interactions have been considered [27] which originate from one designed for neutron rich nuclei [28], but which were

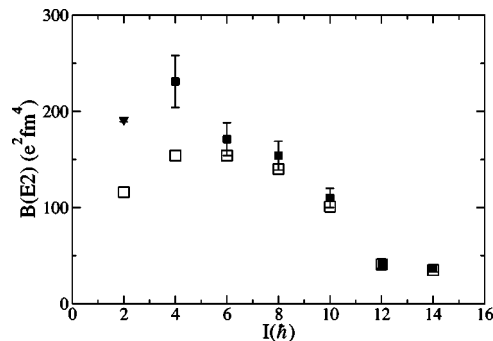


FIG. 7. Experimental $B(E2)$ rates for the gs band in ^{46}Ti as a function of spin: closed squares are from this experiment, closed triangles are from previous data. Theoretical predictions are indicated by open squares.

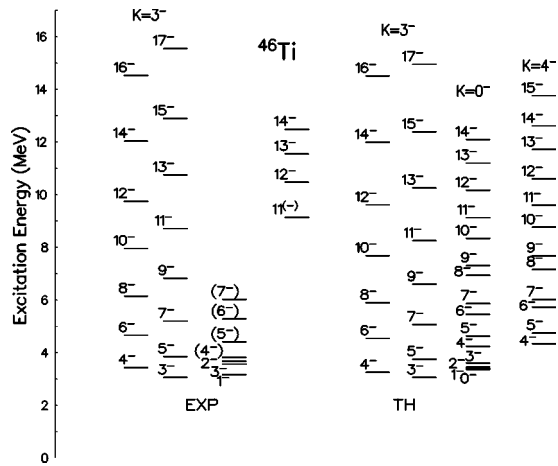


FIG. 8. Comparison of experimental energies for the negative-parity levels and LSSM calculated energies.

also applied in the stable ^{38}Ar [29]. By adopting different versions, the relative position of the predicted lateral bands may change.

In the lower part of Table I experimental data for the $K=3^-$ band are compared with theoretical predictions. In the evaluation of the experimental $B(M1)$ for $\Delta I=1$ transitions the contribution of E2 mixing is neglected, relying on the fact that the subtraction of that component, assuming as reliable the theoretical estimates, would lead to a slightly smaller $B(M1)$ value, inside quoted experimental errors. Experimental and theoretical reduced rates $B(E2)$ and $B(M1)$ of the $K=3^-$ band are compared in Fig. 9. The $B(E2)$ values indicate a larger deformation than predicted. A deformation parameter $\beta \approx 0.25$ is estimated from the transitions between low lying states, i.e., somewhat larger than for the gs band. The $B(M1)$ values inside the $K=3^-$ band are small, both experimentally and theoretically, but, approaching the band

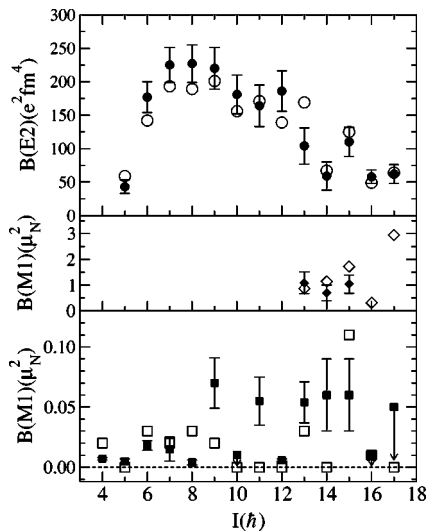


FIG. 9. Reduced transition probabilities as a function of spin for the $K^\pi=3^-$ band of ^{46}Ti . The full and open symbols refer to experimental and theoretical values, respectively. Circles: $B(E2)$ of $I \rightarrow I-2$ transitions; squares: $B(M1)$ of $I \rightarrow I-1$ transitions; diamonds: $B(M1)$ of $I \rightarrow (I-1)_2$ transitions.

termination, the stretched M1 strengths towards yrare levels 14^- , 13^- , and 12^- are very large, in agreement with theory. This indicates the dominance of spherical $\pi d_{3/2} \otimes f_{7/2}^{n+1}$ configurations, in which case $B(M1)$ values 4.51, 0.47, and $0.90 \mu_N^2$ are predicted for transitions $17^- \rightarrow 16_2^-$, $16^- \rightarrow 15_2^-$, and $15^- \rightarrow 14_2^-$, respectively. Such values are similar to the LSSM ones (Table I), but the band spacing regularity is lost. In this context, the M1 transitions connecting the terminating level 17^- with the yrare and the yrast 16^- levels are very different: the former is very large, while the latter is very small. This is explained, considering that, near the terminations, the states of the gs band in ^{47}V and of the $K=3^-$ band in ^{46}Ti can be described with spherical $1f_{7/2}^7$ and $1d_{3/2}^1 \otimes 1f_{7/2}^7$ configurations, respectively. The former and strong transition can be related to the equally strong M1 transition between the terminating levels $29/2^-$ and $31/2^-$ in ^{47}V [3]. Since the terminating level 17^- must be described by coupling the spin of the $1d_{3/2}$ proton-hole parallel with the one of the $31/2^-$ level in ^{47}V , such similarity occurs if the yrare 16^- state originates from the analog parallel coupling with the spin of the yrast $29/2^-$ level. In fact, according to the properties of spherical tensor operators, the spin recoupling caused by the presence of the $1d_{3/2}$ proton-hole gives rise only to a modest variation. The yrast 16^- level, the only further level of such spin built in this configuration space, has to be composed by the unstretched coupling of the ^{47}V $31/2^-$ state with the $1d_{3/2}$ proton-hole. Applying again spherical tensor algebra, the $B(M1)$ value becomes proportional to a linear combination of the static magnetic moments of the proton-hole and the ^{47}V states, with approximate cancellation.

No new information was collected for the non yrast low-lying negative parity levels, reported in the rightmost part of Fig. 1 and compared in Fig. 8 with calculated ones. It is natural to classify those levels, as well as the yrare levels with higher spin, as members of a $K=0^-$ band [11], which can be produced in a similar way as the $K=3^-$ band, but with an antiparallel coupling of the unpaired spins. It has to be noted, however, that the calculated yrare 4^- level has a large positive spectroscopic quadrupole moment, as expected for the head of a $K=4^-$ band. The mixing between the $K=0^-$ and $K=4^-$ bands may explain the rather irregular behavior of the observed sequences. Also other negative parity bands are predicted at little higher energies, but since no new experimental information is presented here, no further discussion will be made.

C. Transitions connecting ^{46}Ti levels with different parity

Several E1 transitions were observed to depopulate the $K=3^-$ band towards the gs band, whose properties are summarized in Table III. The strength of the 97 keV transition from the 3^- level to the yrare 2^+ at 2961 keV is found to be about 100 times smaller than previously reported [8]. The E1 strength of the 1722 keV $14^- \rightarrow 13^+$ transition ($3.9(10) \cdot 10^{-4}$ W.u.) may slightly exceed the adopted limit of $3 \cdot 10^{-4}$ W.u.. In that case it would be the first violation observed in more than one hundred E1 transitions examined in a systematic study in this region [2–6]. The reason for the comparatively enhanced E1 decay between some states ap-

TABLE IV. Lifetimes in the gs bands of ^{48}Cr and ^{50}Cr . The values refer to the upper level of the transition.

Transition $I_i^\pi \rightarrow I_f^\pi$	E_γ (keV)	τ_{exp} present (ps)	τ_{exp} previous (ps)	τ_{th} (ps)
^{48}Cr				
$4^+ \rightarrow 2^+$	1106	1.74(18)	1.5(5), ^a 1.9(5) ^b	1.59
$2^+ \rightarrow 0^+$	752		10.3(11) ^b	15.4
^{50}Cr				
$4^+ \rightarrow 2^+$	1098	2.12(23)	2.5(7), ^a 3.2(4) ^b	1.9
$2^+ \rightarrow 0^+$	783		12.5(7) ^c	14.6

^aReference [1].^bReference [30].^cReference [31].

proaching band termination in the band $K=3^-$ towards the gs band may be that the excitation energy is sufficient to excite a $1d_{5/2}$ nucleon. A small contribution of $\pi d_{5/2}^{-1} \otimes f_{7/2}^{n+1}$ configuration would allow an E1 transition from the $1f_{7/2}$ to the $1d_{5/2}$ orbital. A similar effect could be due to the $1g_{9/2}$ orbital but is probably less important since an E1 enhancement is not observed in heavier nuclides.

It should be noted, moreover that the yrare 0^+ at 2611 keV decays to the 2^+ via a 1722 keV line which may get rise to some contamination.

A branch from the 3^- level to the ground state was observed, which corresponds to a noncollective E3 transition. A mixed M2+E3 decay has been observed, which connects the 4^- level at 3441 keV to the 2^+ one at 889 keV. This provides an upper limit for the M2 strength, which turns out to be retarded as usually.

D. ^{48}Cr and ^{50}Cr

The results for ^{48}Cr and ^{50}Cr are presented in Table IV. The value presently obtained for the lifetime of the 4^+ level in ^{50}Cr is sensibly lower than that measured with the RDDS method [31]. This may be due to the fact that in that measurement the feeding time was not explicitly accounted for. The extracted B(E2) values for the $4^+ \rightarrow 2^+$ transitions agree with theoretical values. The only marked disagreement is

that the B(E2) rate of the $2^+ \rightarrow 0^+$ transition in ^{48}Cr is considerably larger than that calculated with LSSM [1]. This resembles the situation found for the 2^+ state in ^{46}Ti and could be related to some mixing with a 2- and 4-hole configuration. Deformation parameters $\beta \approx 0.24$ and 0.26 are deduced for ^{50}Cr and ^{48}Cr , respectively.

V. CONCLUSIONS

The spectroscopy of ^{46}Ti , lying in the middle of the $1f_{7/2}$ shell, has been greatly extended through the determination of electromagnetic transition rates. In order to get reliable DSAM lifetimes, the stopping power for the recoil in Au and Pb was preliminarily investigated.

The observed B(E2) enhancement in the gs band points to the build up of rotational collectivity. LSSM calculations in the full pf shell predict well the energies and electromagnetic moments of the gs band from $I^\pi=6^+$, up to the $I^\pi=14^+$ band termination in the $f_{7/2}$ shell. The predictions are poor for lower spin states, yrast or not, due to the admixture of deformed 2 and 4 hole configurations from the sd shell which are not taken into account.

Concerning the $K=3^-$ band, the main features, as well as the E2 and M1 transitions, are well reproduced up to the $I^\pi=17^-$ band termination by extending the configuration space to include one hole in the $1d_{3/2}$ orbital. The enhanced M1 decay of the 13^- , 14^- , and 15^- levels toward a sideband is also predicted.

LSSM predicts many negative parity levels, which can be organized in bands, whose relative position strongly depends on the fine tuning of the residual interaction. This is a challenge for further experiments aimed to a ‘‘full spectroscopy.’’

Good agreement with theory is also found for the lifetimes of 4^+ levels in ^{48}Cr and ^{50}Cr . The deduced deformation of the gs band ^{50}Cr turns out to be somewhat larger than in the cross-conjugate in ^{46}Ti , while the maximum deformation is observed in ^{48}Cr , even if slightly smaller than previously suggested [1].

ACKNOWLEDGMENTS

J.R.B.O., N.H.M., and R.V.R. would like to acknowledge financial support from the Brazilian agencies CNPq (Conselho Nacional de Desenvolvimento Científico e Tecnológico) and FAPESP (Fundação de Amparo à Pesquisa do Estado de São Paulo), and INFN (Italy).

[1] F. Brandolini *et al.*, Nucl. Phys. **A642**, 387 (1998).
 [2] F. Brandolini *et al.*, Phys. Rev. C **60**, 041305 (1999).
 [3] F. Brandolini *et al.*, Nucl. Phys. **A693**, 517 (2001).
 [4] F. Brandolini *et al.*, Phys. Rev. C **64**, 044307 (2001).
 [5] F. Brandolini *et al.*, Phys. Rev. C **66**, 024304 (2002).
 [6] F. Brandolini *et al.*, Phys. Rev. C **66**, 021302 (2002).
 [7] E. Caurier, J. L. Egido, G. Martínez-Pinedo, A. Poves, J. Retamosa, L. M. Robledo, and A. P. Zuker, Phys. Rev. Lett. **75**, 2466 (1995).

[8] S.-C. Wu, Nucl. Data Sheets **91**, 1 (2000).
 [9] D. Bucurescu *et al.*, Phys. Rev. C **67**, 034306 (2003).
 [10] J. A. Cameron *et al.*, Phys. Rev. C **58**, 808 (1998).
 [11] F. Brandolini *et al.*, LNL Annual Report 2001, p. 12.
 [12] O. Möller, K. Jessen, A. Dewald, A. F. Lisetskiy, P. von Brentano, A. Fitzler, J. Jolie, A. Linnemann, B. Saha, and K. O. Zell, Phys. Rev. C **67**, 011301 (2003).
 [13] G. D. Dracoulis, D. C. Radford, and A. R. Poletti, J. Phys. G **4**, 1323 (1978).

- [14] F. Brandolini *et al.* (unpublished).
- [15] J. A. Cameron, M. A. Bentley, A. M. Bruce, R. A. Cunningham, W. Gelletly, H. G. Price, J. Simpson, D. D. Warner, and A. N. James, *Phys. Rev. C* **44**, 1882 (1991).
- [16] J. C. Wells and N. Johnson, Report No. ORNL-6689 (1991), p. 44.
- [17] L. C. Northcliffe and R. F. Schilling, *At. Data Nucl. Data Tables* **A7**, 233 (1970).
- [18] S. H. Sie, D. Ward, J. S. Geiger, R. L. Graham, and H. R. Andrews, *Nucl. Phys.* **A291**, 443 (1977).
- [19] F. Brandolini and R. V. Ribas, *Nucl. Instrum. Methods Phys. Res. A* **417**, 150 (1998).
- [20] A. Poves, J. Sánchez-Solano, E. Caurier, and F. Nowacki, *Nucl. Phys.* **A694**, 157 (2001).
- [21] W. A. Richter, M. G. Van Der Merwe, R. E. Julies, and B. A. Brown, *Nucl. Phys.* **A523**, 325 (1991).
- [22] W. J. Gerace and A. M. Green, *Nucl. Phys.* **A113**, 641 (1968).
- [23] C. D. O'Leary, M. A. Bentley, B. A. Brown, D. E. Appelbe, R. A. Bark, D. M. Cullen, S. Ertürk, A. Maj, and A. C. Merchant, *Phys. Rev. C* **61**, 064314 (2000).
- [24] K. E. G. Löbner, M. Vetter, and V. Höning, *At. Data Nucl. Data Tables* **7**, 495 (1970).
- [25] W. Kutschera, B. A. Brown, and K. Ogawa, *Riv. Nuovo Cimento* **I**, 12 (1978).
- [26] A. Poves and J. Sanchez-Solano, *Phys. Rev. C* **58**, 179 (1998).
- [27] S. Nummela *et al.*, *Phys. Rev. C* **63**, 044316 (2001).
- [28] J. Retamosa, E. Caurier, F. Nowacki, and A. Poves, *Phys. Rev. C* **55**, 1266 (1997).
- [29] D. Rudolph *et al.*, *Phys. Rev. C* **65**, 034305 (2002).
- [30] L. P. Ekström, G. D. Jones, F. Kearns, T. P. Morrison, O. M. Mustaffa, D. N. Simister, H. G. Price, P. J. Twin, R. Wadsworth, and N. J. Ward, *J. Phys. G* **5**, 803 (1979).
- [31] W. Dehnhardt, O. C. Kistner, W. Kutschera, and H. J. Sann, *Phys. Rev. C* **7**, 1471 (1973).